Hydration of Na+, Ni2+, and Sm3+ in the Interlayer of Hectorite: A Quasielastic Neutron Scattering Study

Oleg S. Sobolev, Lydie Le Forestier, Miguel A. Gonzales, Laurent Charlet

Hydration of Na^{+}, Ni^{2+}, and Sm^{3+} in the interlayer of hectorite: a quasielastic neutron scattering study

Oleg Sobolev[1*], Lydie Le Forestier[2], Miguel A. Gonzalez[3], Margarita Russina[4], Ewout Kemner[4], Gabriel J. Cuello[3], and Laurent Charlet[1]

[1]LGIT, University of Grenoble and CNRS, BP53, 38041 Grenoble, France

[2]Université d'Orléans, CNRS/INSU, Université de Tours, Institut des Sciences de la Terre d'Orléans, 1A rue de la Férollerie, 45071 Orléans Cedex 2, France

[3]Institut Laue Langevin, 6 rue Jules Horowitz, BP 156, 38042 Grenoble Cedex 9, France

[4]Helmut-Zentrum Berlin für Materialien und Energie, Glienicker Strasse 100, D-14109 Berlin, Germany

*Corresponding author. E-mail: sobolev38@gmail.com

Abstract

Quasielastic neutron scattering experiments were performed with Na-hectorite, Ni-hectorite, and Sm-hectorite samples in order to find out whether Sm^{3+} is present in the clay interlayer as a fully hydrated cation (outer-sphere complex), or, as it follows from neutron diffraction data analysis, it is dehydrated and bound to the clay surface (inner-sphere complex). The results obtained for the Sm-hectorite were compared with other interlayer cations: strongly hydrated Ni^{2+} and relatively weakly hydrated Na+. It was found that water mobility in the Sm-hectorite sample is very close to the water mobility in Ni-hectorite. This is only possible if the Sm^{3+} ion is fully hydrated. It was shown that water molecules hydrating Ni^{2+} and Sm^{3+} exhibit diffusion

mobility measurable with backscattering spectrometers. The diffusion coefficients of the exchangeable cations were found using the slow exchange approximations D_{Ni} = (0.05 – 0.14) x 10^{-9} m^2/s and D_{Sm} = (0.04 – 0.18) x 10^{-9} m^2/s.

1. Introduction

Smectite clay minerals are layer-type aluminosilicates, which are ubiquitous on our planet in geologic deposits, terrestrial weathering environments, and marine sediments. They consist of negatively charged silicate layers held together by cations to give a stacked (crystalline) structure. Under humid conditions, the cations in the interlayer and the internal clay surfaces are hydrated. Due to their hydration ability and charged layers, smectites possess important properties such as swelling ability, low hydraulic conductivity, good plasticity, and both high cation-exchange and adsorption capacities - all of which make them very useful for several applications. For instance, clay minerals are widely used in the various industries as a viscous gelling or a clarifying agent. Smectites are intensively used in environmental contexts including their applications in waste confinement barriers. Furthermore, clay minerals have been selected as the most suitable buffer material for high-level radioactive waste repositories. The buffer material is expected to retard the migration of the radionucleides in the case of corrosion of the waste package material.

Cation adsorption complexes can be classified as either inner-sphere or outer-sphere. An inner-sphere surface complex has no water molecule interposed between the clay surface and the cation, whereas an outer-sphere surface complex has at least one such interposed water molecule. Outer-sphere surface complexes thus comprise fully hydrated cations [1].

Among the radionucleides that could be potentially released from radioactive waste repositories and then migrate through the clay barrier, the trivalent cations represent an important part. The lanthanides are of interest because they are often taken as a chemical analog for trivalent actinides [2]. The results for Nd^{3+}- and Yb^{3+}- exchanged Wyoming montmorillonite obtained by means of neutron diffraction with isotopic substitution were reported in ref 3. It was found that Nd^{3+} and Yb^{3+} are only partially hydrated and are bound to the clay surface probably as a result of heat treatment at 100^{o}C during sample preparation. It was supposed that this treatment was sufficient to cause the lanthanide ions to dehydrate and to bind irreversibly to the clay surface oxygen atoms.

In a previous experiment [4,5], we studied by means of neutron diffraction with isotopic substitution the structural parameters of the coordination of Sm^{3+}, adsorbed in the interlayer space of the montmorillonite. It was found that the number of hydrogen atoms, $N_H = 5.5 \pm 2.0$, in the first coordination shell of Sm^{3+} is equal or even slightly smaller than those of oxygen atoms, $N_O = 7.5 \pm 1.0$. This means that not all these oxygen atoms belong to water molecules. It was supposed that the Sm^{3+} ion binds to the clay surface via oxygen siloxane atoms (forms an inner-sphere complex), and it is probably partially hydrolyzed. This result is very close to those obtained earlier for Yb^{3+} and Nd^{3+}, although the sample preparation methods and sample mineralogy differ for the two studies. Recently we performed a neutron diffraction experiment with the hydrated Sm – synthetic hectorite samples [6], and obtained the numbers: $N_O = 7.5 \pm 1$ and $N_H = 8.5 \pm 2$. Though the N_H value obtained for Sm – synthetic hectorite is slightly higher than in montmorillonite, again, it is much smaller than the value expected for the fully hydrated cation.

On the other hand, results obtained by other spectroscopic methods do not support the hypothesis that the lanthanide cations form inner-sphere complexes with the clay surface: those cations were found to be localized at the middle of the clay interlayer, fully hydrated, indicating outer-sphere complexation [3,7,8].

The aim of the present work was to carry out a quasielastic neutron scattering (QENS) experiment with hydrated Sm-smectite and to compare QENS results obtained for Sm^{3+} with other interlayer cations: strongly hydrated Ni^{2+} and relatively weakly hydrated Na^{+}.

In this type of study, the Na-smectite and Ni-smectite systems are very well studied, and they can be used as “reference” samples. It is known from the neutron diffraction experiments that the hydration structure of the Ni^{2+} ion in clay interlayer is very close to that in aqueous solution. Like in aqueous solution, the number of water molecules in the first coordination shell of interlayer Ni^{2+} cation is equal to 6 [9]. The hydration enthalpy of Ni^{2+} in solutions is $\Delta H°_{hyd} = -2105$ kJ mol^{-1} [10]. According to QENS data, the Ni^{2+}-water binding time is $\tau > 10^{-9}$ s [11] in aqueous solution, whereas the NMR gives $\tau \sim 10^{-6}$ s [12]. This time is very long in comparison with the observation time for the QENS experiment and, therefore, the QENS spectra for the hydrated Ni-smectite should contain two distinct components: one corresponding to the water molecules hydrating Ni^{2+} cation (bound water) and another one for the other water molecules (“free” water). The term “free” is hardly applicable to the water molecules in the clay interlayer, but we will use it just for brevity’s sake.

The Na^{+}-water interaction is much weaker ($\Delta H°_{hyd} = -409$ kJ mol^{-1} [10]) and, the estimation for the binding time τ is 10 to 20 ps [13,14]. Thus the molecules in the hydration

shell should be in a fast exchange regime (see section 2.3) with other molecules (one can say the same on the molecules hydrating the clay surface), and QENS can be considered in the single component approximation. The QENS experiments reveal diffusion coefficient of water molecules in Na-montmorillonite to be $D \sim 10^{-9}$ m^2 s^{-1} [15,16] which is comparable to that of bulk water (2.3×10^{-9} m^2 s^{-1}).

Thus in the case of a dehydrated Sm^{3+} cation bound to the clay surface, the result should be similar to that of Na-smectite. In the case of fully hydrated Sm^{3+} cation ($\Delta H°_{hyd}$ = -3449 kJ mol^{-1} [10]), the scattering pattern should be close (at least qualitatively) to that of Ni-smectite.

Since the maximal amount of cations that can be adsorbed in the clay interlayer is in inverse proportion to their charge, and assuming that the cations to be fully hydrated like in solution (hydration numbers 6 for Ni^{2+} and 9 for Sm^{3+}), the number of water molecules interacting with interlayer cations should be roughly the same in clay samples fully saturated with either Sm or Ni ($N_{Sm} \times N_{H20}^{hyd} \sim 1/3 \times 9 = 3$; $N_{Ni} \times N_{H20}^{hyd} \sim ½ \times 6 = 3$).

For our experiment, we used synthetic hectorite, in which the structural OH groups were replaced by F atoms. This opens the new great possibilities for the QENS study of water dynamics in clay, making it possible to explore subtle effects of hydration that, in the case of natural clays, are hidden under the strong elastic peak originated from the clay structural hydrogen atoms. This material has also other advantages in comparison with natural clays; namely very well-defined structure and charge distribution on the clay layers, leading to a highly regular swelling [17], in contrast to its natural counterparts.

In Section 2 of this paper, the general description of the QENS is given, and the problems of the QENS data analysis for hydrated clay samples are discussed. In this section, we also consider the fast and slow exchange limits of the QENS that are very important for the systems containing different classes of diffusing particles. Section 3 describes samples preparation, chemical analysis and QENS experiments. The experimental results are examined in Section 4. First we start with a preliminary analysis using the simplest models, then in the second part of Section 4 we analyze the data obtained for Ni-hectorite and Sm-hectorite samples in more detail using the slow exchange limit approximation. In Section 5 we summarize the conclusions.

2. Models and Methods

2.1. Basics

The scattering law *S(Q,ω)* measured in an inelastic neutron experiment is the distribution of neutrons that have undergone an energy exchange $\hbar\omega = E_i - E_f$, and a wave vector transfer, $\vec{Q} = \vec{k}_i - \vec{k}_f$, after scattering by the sample. Scattering from water is dominated by the scattering cross-section for hydrogen, which is over 98% incoherent. In the incoherent approximation *S(Q,ω)* is connected with the Van Hove self-correlation function $G_s(\vec{r},t)$ via a double Fourier transform in space and time [18,19]:

$$S(\vec{Q},\omega) = \frac{1}{2\pi}\iint G_s(\vec{r},t)\exp\left(i(\vec{Q}\vec{r} - \omega t)\right)d\vec{r}\,dt \qquad (1)$$

In the classical limit $G_s(\vec{r},t)$ is defined as the probability of finding a particle at a position $\vec{r}$ at a time *t* when the same particle was at the origin at time *t = 0*.

For the modeling of *S(Q,ω),* it is often convenient to use the intermediate scattering function *I(Q,t)*:

$$I(Q,t) = \int G_s(\vec{r},t)\exp(\vec{Q}\vec{r})d\vec{r} = \left\langle \exp\left(-i\vec{Q}\vec{r}_j(0)\right)\exp(i\vec{Q}\vec{r}_j(t))\right\rangle, \qquad (2)$$

where angular brackets denote ensemble average, and *r(0)* and *r(t)* are, respectively, the coordinate of a particle at *time 0* and the coordinate of the same particle at *time t*.

Thus the scattering law *S(Q,ω)* can be expressed by the following expression:

$$S(\vec{Q},\omega) = \frac{1}{2\pi}\int I(\vec{Q},t)\exp(-i\omega t)dt \qquad (3)$$

In the case of liquid sample, at infinite time, the scattering particle can access any coordinate in space, independently of its initial position, and *I(Q,t)* tends to zero at $t \to \infty$. If the motion of the particle is well located in space (atoms in the crystal), or restricted to a particular volume (diffusion in confined space, molecular reorientations) *I(Q,t)* tends to a nonvanishing value $I(Q,\infty)$. Therefore, in the most general case, *I(Q,t)* can split into its asymptotic value in the long-time limit $I(Q,\infty)$ and the time-dependent part $I_{inel}(Q,t)$ according to

$$I(Q,t) = I(Q,\infty) + I_{inel}(Q,t), \qquad (4a)$$

and the scattering law can be expressed [18,19]:

$$S(\vec{Q},\omega) = I(\vec{Q},\infty)\delta(\omega) + \frac{1}{2\pi}\int I_{inel}(\vec{Q},t)\exp(-i\omega t)dt \qquad (4b)$$

The delta function $\delta(\omega)$ in this expression represents elastic scattering; it is absent in the case of liquid sample because of long-range translational diffusion of the molecules. In our particular case of a clay sample, elastic scattering arises from clay atoms that, in the long

time limit, can be considered as immobile. The second term is inelastic scattering corresponding to any kind of molecular motions.

It is generally assumed that different kinds of motions are uncorrelated and the incoherent intermediate scattering function in the long time limit corresponding to QENS has the form:

$$I_{inel}(Q,t) \approx I_{q.el.}(Q,t) = I_{tr}(Q,t) I_r(Q,t) \exp(-2W) \quad (5)$$

where the exponent is the Debye-Waller factor, $I_{tr}(Q,t)$ and $I_r(Q,t)$ represent the contributions from the translational and the low-frequency rotational motions respectively. This supposition is not always correct, nevertheless, it is widely used in order to have a tractable analytical model for the data analysis.

$I_{tr}(Q,t)$ tends to zero at $t \to \infty$, whereas the reorientation function $I_r(Q,t)$ is a sum of its asymptotic value in the long-time limit $I_r(Q,\infty)$ and the time-dependent part $I_{rqel}(Q,t)$:

$I_r(Q,t) = I_r(Q,\infty) + I_{rqel}(Q,t)$

and the quasielastic scattering law can be expressed as [18,19]:

$$S_{qel}(Q,\omega) = \left(EISF(Q) S_{tr}(Q,\omega) + S_{tr}(Q,\omega) \otimes S_{rqel}(Q,\omega)\right) \exp(-2W) \quad (6)$$

where the sign $\otimes$ denotes the convolution operation, $S_{tr}(Q,\omega)$ and $S_{rqel}(Q,\omega)$ are Fourier transforms of $I_{tr}(Q,t)$ and $I_{rqel}(Q,t)$ correspondingly. $EISF(Q) = I_r(Q,\infty)$ is the elastic incoherent structure factor characterizing the geometry of the rotation [18,19].

The simplest models for the diffusion motion predict an exponential form for the translation diffusion function:

$$I_{tr}(Q,t) = \exp(-\Gamma(Q)t) \quad (7a)$$

that corresponds to the Lorentzian form of the scattering law $S(Q,\omega)$:

$$S(\vec{Q},\omega) = \frac{1}{\pi} \frac{\Gamma(Q)}{\Gamma^2(Q) + \omega^2}, \quad (7b)$$

where $\Gamma(Q)$ is the half-width at half maximum of the quasielastic peak. At low Q values, $\Gamma(Q)$ tends to the limit, corresponding to the simple diffusion (Fick's law):

$$\Gamma(Q) = DQ^2 \quad (8)$$

At higher Q, different models [18,19] predict deviation from the Fick's law and suppose a jumping mechanism of diffusion.

The models for rotation motion describe generally $I_{rqel}(Q,t)$ by the infinite series of exponential functions, but in practice, depending on Q range, the three (or less) first terms of the expansion are quite enough for the data analysis. The characteristic times of these

exponents, in contrast to $I_{tr}(Q,t)$, do not depend on Q [18,19]. The Sears' model describes the isotropic rotational diffusion:

$$S_{rot}(Q,\omega) = EISF(Q)\cdot\delta(\omega) + S_{rqel}(Q,\omega) =$$
$$j_0^2(QR_0)\cdot\delta(\omega) + \sum_{\ell=1}^{\infty}(2\ell+1)j_\ell^2(QR_0)\cdot\frac{1}{\pi}\frac{\ell(\ell+1)D_r}{(\ell(\ell+1)D_r)^2+\omega^2}, \quad (9)$$

Here R_0 is the radius of rotation, D_r is the rotation diffusion constant, j_l are the spherical Bessel functions.

Thus, in the framework of the "traditional" approach, the quasielastic spectra are usually approximated by a sum of a few Lorentzian functions corresponding to the translational and rotational motions. The Lorentzian shape of the quasielastic components $S(Q,\omega)$ is defined by the simple exponential decay of the corresponding $I(Q,t)$ functions.

It was found, however, for supercooled liquids, glasses, polymers, proteins, and some other substances that diffusive and reorientational relaxation processes in these systems deviate from the exponential form and can be described by the stretched exponent (Kohlrausch-Williams-Watt function (KWW)) [20,22]:

$$KWW(t) = \exp(-(t/\tau_w)^\beta) \quad (10)$$

The reasons for such a behavior can be different for different systems. Two limiting scenarios are invoked to explain KWW functional form: "homogeneous" and "heterogeneous" scenarios [20,21]. According to the "heterogeneous" scenario, the KWW function is a superposition of different simple exponential relaxations weighted by a broad distribution of relaxation times. The "homogeneous" scenario supposes that all of the particles in the system relax nonexponentially. In the case of "homogeneous" non-exponential behavior, the shape parameter β is considered as an indicator of the degree of correlation or cooperativity of the relaxation process.

2.2. Water diffusion in clays. Methods of QENS analysis.

In spite of previous extensive studies of water microscopic dynamics in the interlayer of montmorillonite [15,16,23,24] and vermiculite [25-28] by QENS, there is no full agreement about the method to be used for data analysis. Both methods, supposing Lorentzian shape of the $S(Q,\omega)$ (exponential decay of $I(Q,t)$) and based on the KWW form of $I(Q,t)$, have been used for the analysis of water mobility in the clay interlayer space.

There is experimental evidence that water diffusion mobility is a complex dynamical process that cannot be described with the use of a single characteristic time. The diffusion coefficients and residence times of water molecules measured with high resolution (neutron

spin-echo (NSE), backscattering) and low resolution (time-of-flight (TOF) spectroscopy) show a significant difference [15,23,25-28]. For example, Swenson et al. [25-28] investigated the dynamics of confined water in a fully hydrated Na-vermiculite clay using the NSE and the TOF technique. It was found that the diffusion constant obtained using the NSE is about 40 times lower than the result of the TOF experiment. They also reported the very stretched behavior of the *I(Q,t)* function, supposing that this behavior can be interpreted as evidence for a broad distribution of relaxation times, probably because the water molecules have widely different local environments. Malikova et al. [15] reported an evident difference between NSE and TOF results obtained for Na- and Cs-montmorillonite samples. On the other hand, the same research team reported a good agreement in the relaxation times of water mobility in a synthetic Na-hectorite extracted with the NSE and TOF techniques using monoexponential approximation for *I(Q,t)* function [17].

Water mobility in clay interlayer is strongly anisotropic; it is suppressed in the direction perpendicular to the clay platelets. In the case of a nonoriented powder sample, the experimental QENS reflects the two-dimensional water diffusion averaged over all possible directions of the clay particles. Supposing that water diffusion can be described by the diffusion coefficient parallel to the clay layers $D_{||}$ (low Q limit, eq. 8), and *I(Q,t)* is exponential (eq. 7), the powder average can be written as follows [17]:

$$\left\langle I_{2d}(\vec{Q},t)\right\rangle_{\theta} = \frac{1}{2}\int_{0}^{\pi} \exp(-D_{||}Q^{2}\sin^{2}(\theta)\,t)\sin\theta\, d\theta \qquad (11)$$

where θ is the angle between the wavevector $\vec{Q}$ and the direction perpendicular to the clay layers. It was shown that this powder average affects the shape of the QENS signal, resulting in the deviation of the experimental *I(Q,t)* from the exponential form. Moreover, it was found [17] that the analysis of the data in an isotropic approximation underestimated the diffusion coefficient of the interlayer water molecules by 25 %. Strictly speaking, eq. 11 is only valid for low water content (monolayer). In the case of higher water content (double layer and higher), one should take into account the diffusion coefficient $D\perp$ in the direction perpendicular to the clay layers. This leads to a more complicated expression for the experimental *I(Q,t)* and *S(Q,ω)* [29]. However, the use of that expression for fitting the data obtained for a powder sample is problematic because of the strong correlation between $D_{||}$ and $D\perp$ parameters.

2.3 Fast and slow exchange limits of QENS

For a proper analysis of QENS results, one should take into account the fact that the clay interlayer contains different types of water molecules: water molecules hydrating the exchangeable cations, and water molecules interacting only with other water molecules and clay surface. The water molecules can undergo transitions between these types. If this exchange is slow, the QENS spectra contain distinct components with different characteristic times (widths) corresponding to different types of water molecules (slow exchange limit). In the case of the fast exchange, only a single population of water molecules with averaged diffusion mobility can be observed in the experiment.

Salmon [30] considered the system containing two classes of molecules with the mean lifetime τ_i and molecular fraction n_i in class i (=1,2). The diffusion of the particles was described by the diffusion coefficients D_i, corresponding to the low Q limit of the neutron scattering experiment (eq. 8). It was found that the fast exchange limit takes place when $\tau_i << 1/D_iQ^2$. In this case, $S(Q,\omega)$ is a single Lorentzian. In the slow exchange limit, that is, when $\tau_i >> 1/D_iQ^2$, the exchange between classes is relatively slow, and the scattering law is the sum of two weighted Lorentzian functions.

The formulas, analogous to those presented in ref 30, can be derived assuming that $I_i(Q,t)$ can be approximated by the exponential $I_i(Q,t) \approx \exp(-\Gamma_i(Q)t)$ (see Supporting Information). Again, if $n_2\tau_1 << 1/\Gamma_1(Q), 1/\Gamma_2(Q)$, the scattering law $S(Q,\omega)$ is the single Lorentzian

$$S(Q,\omega) = \frac{1}{\pi}\frac{\overline{\Gamma(Q)}}{\overline{\Gamma(Q)}^2 + \omega^2}, \text{ where } \overline{\Gamma(Q)} = n_1\Gamma_1(Q) + n_2\Gamma_2(Q) \qquad (12a)$$

In the slow exchange limit, when $n_2\tau_1 >> 1/\Gamma_1(Q), 1/\Gamma_2(Q)$, the $S(Q,\omega)$ is the sum of two weighted Lorentzian functions:

$$S(Q,\omega) = \frac{1}{\pi}\left(\frac{n_1\Gamma_1(Q)}{\Gamma_1^2(Q) + \omega^2} + \frac{n_2\Gamma_2(Q)}{\Gamma_2^2(Q) + \omega^2}\right) \qquad (12b)$$

Expressions 12a and 12b are more universal because they do not suppose any explicit form of $\Gamma_i(Q)$, thus they can be used for higher Q values, where $\Gamma_i(Q)$ deviates from the simple diffusion law (eq. 8).

However, this approach is applicable for more general cases as well, although exact mathematical expressions can be obtained for the simplest cases only. The argument for the most general case is the following: The $I(Q,t)$ function of the system that contains two classes of molecules can be presented as

$$I(Q,t) = n_1\tilde{I}_1(Q,t) + n_2\tilde{I}_2(Q,t) \qquad (13)$$

where $\widetilde{I}_i(Q,t)$ corresponds to the particles that are in the *i*th class at the moment *t = 0*: $\widetilde{I}_i(Q,t=0) = I_i(Q,t=0) = 1$, *$I_i(Q,t)$* describes the scattering from the particles of the *i*th class [30]. The molecules can change their class, and in general case, $\widetilde{I}_i(Q,t \neq 0) \neq I_i(Q,t \neq 0)$, so that the function $\widetilde{I}_i(Q,t)$ describes the motions of the molecule in a mixed state. Because of diffusion of the particles, the functions *I(Q,t)* describing QENS decay to *0* at $t \to \infty$. We can introduce the decay time τ_i^D of $\widetilde{I}_i(Q,t)$ as the time when $\widetilde{I}_i(Q,\tau_i^D) << \widetilde{I}_i(Q,0)$, and the integral (eq. 3) can be approximated as

$$S(\vec{Q},\omega) \approx \frac{1}{2\pi}\int_{-\tau_i^D}^{-\tau_i^D} I(\vec{Q},t)\exp(-i\omega t)dt \qquad (14)$$

If $\tau_i << \tau_i^D$ the system is in the fast exchange limit, and then no matter where the molecule was at the moment *t = 0*, $\widetilde{I}_1(Q,t) \approx \widetilde{I}_2(Q,t)$. If the transitions are rare, $\tau_i >> \tau_i^D$, $\widetilde{I}_1(Q,t) \approx I_1(Q,t)$ and $\widetilde{I}_2(Q,t) \approx I_2(Q,t)$. The decay time τ^D can be roughly estimated as $\tau^D \sim$ *1/Γ(Q)*.

Thus in a QENS experiment, the ability to see the difference between different types of particles, such as water molecules hydrating cations and other molecules, depends on the mobility of these molecules. However, in a real experiment, the behavior of the *I(Q,t)* function cannot be observed at the time *t* longer than the observation time τ_{obs} defined by the instrumental resolution $\tau_{obs} \sim 1/\Delta_{res}$, Δ_{res} is the full width at half-maximum (fwhm) of the resolution function of the spectrometer. Therefore the sufficient condition for the slow exchange limit can be written as $\tau_i >> \tau_{obs}$.

3. Experiment

3.1 Sample preparation and characterization

A fluorated hectorite used for all sample preparations was firstly synthesized at the University of Orleans, by using the procedure [31] adapted from the conventional gelling method of Hamilton and Henderson [32]. The chemical formulas of the synthetic hectorite is $Na_{0.8}(Mg_{5.2}Li_{0.8})Si_8O_{20}F_4.nH_2O$ per unit cell. Concerning the gel preparation, all chemicals had 99% minimum grade purity. At first, Li_2CO_3 and Na_2CO_3, dried at 105°C, were added to a $Mg(NO_3)_2.6H_2O$ solution (titration of 102.5 mg MgO/g) with a few drops of nitric acid, to

complete the dissolution of the carbonates (pH=2). A similar volume of ethanol used as solvent was poured into this aqueous solution, and tetraethylorthosilicate (TEOS) was added as the silicon source. A precipitate was obtained by neutralizing the resulting solution by addition of NH_4OH. After the complete hydrolysis (16 h), this gel was dried and progressively heated to 600°C to remove water, organic matter, NO_2, and CO_2, and to obtain a Na-Mg-Li-Si oxide gel. An appropriate quantity of dried MgF_2 was added, and the resulting gel was finally ground in an agate mortar. Experimental charges were placed into gold capsules, which were after that closed by arc-welding. Hydrothermal syntheses were carried out in Tuttle-type, externally heated, cold-seal pressure vessels, using argon as the pressure medium at 350°C and 50 MPa, for a run duration of 28 days. All capsules were checked for leakage before the experiment (test with oil), and after by reweighing.

For the preparation of the Sm-hectorite sample we used the isotope ^{154}Sm in order to reduce the neutron adsorption, which is very high for natural Sm. The Na-hectorite was suspended in 0.05M solution of Sm^{3+} at pH = 4 and left with stirring. After 2 days of equilibration the suspension was filtered and dried at room temperature. The Sm content in the filtered solution was analyzed using ICP-OES. It was found that 97% of Sm was adsorbed in the clay, and the concentration of Sm in the dry clay (taking into account the water content in the sample) was 0.356 mmol/g. This value corresponds to the charge of 0.84*e* per unit cell, which is slightly higher than the nominal value 0.8*e*.

The Ni-hectorite sample was prepared by suspending the Na-hectorite in 0.05M $NiCl_2$ solution at pH = 4 and then left with stirring for 24 h. The clay was separated from the solution by centrifugation, and the procedure was repeated three times. Finally the suspension was filtered and washed with distilled water in order to remove the excess salt.

The dry powder Na-hectorite, Ni-hectorite, and Sm-hectorite samples were kept in a humid atmosphere at relative humidity (RH) = 85% fixed by saturated KCl solution for 3 weeks. For the water content analysis, 200mg portions of the samples were dried in the oven at 150 ^oC for 3 days. The water contents for all three samples were found to be almost the same and equal to $M_{H2O}/M_{dryclay} \approx 0.21 \pm 0.01$. This value corresponds to 9.2 water molecules per unit cell (two-layer hydrate). The nominal composition of the three samples is given then by the following unit cell formulas:

$$Na_{0.8}(Mg_{5.2}Li_{0.8})Si_8O_{20}F_4 - 9.2\ H_2O \quad (15a)$$

$$Ni_{0.4}(Mg_{5.2}Li_{0.8})Si_8O_{20}F_4 - 9.2\ H_2O \quad (15b)$$

$$Sm_{0.28}(Mg_{5.2}Li_{0.8})Si_8O_{20}F_4 - 9.2\ H_2O \quad (15c)$$

Formula 15c shows the total concentration of Sm adsorbed in the clay mineral. However, for a proper QENS data analysis, it is important to know the number of cations that interact with water molecules. This number can be less than the total amount of adsorbed Sm due to concurrent chemical reactions in the sample, such as precipitation. At pH = 4 the dominant samarium species in aqueous solution is Sm^{3+}, and cationic exchange is the main mechanism of adsorption in the clay mineral at this pH value [2]. However, this acidity was measured for the bulk clay suspension, and it could be changed during preparation of the powder sample for the experiment: drying and equilibration with a humid atmosphere.

A cationic exchange analysis was done with the Sm-hectorite and Ni-hectorite samples after the neutron scattering experiments. The aim of this analysis was to find how much of adsorbed Sm and Ni is readily exchangeable and therefore persists in the clay interlayer in the cationic form. The Sm-hectorite and Ni-hectorite samples were placed into concentrated CsCl solution at pH = 4 for several hours. After centrifugation, the solution was changed, and the old solution was kept for analysis in a separate tube. The procedure was repeated four times. At the end for each sample, we had four tubes with the solutions containing Ni^{2+} or Sm^{3+} that were replaced by Cs^{+} in the clay mineral. The concentrations of Sm^{3+} and Ni^{2+} in these solutions were analyzed by ICP-OES, and the results are shown in Figure 1. The amount of the cations released from the samples in the solution decreased very rapidly with the number of the solution replacement procedures (i.e., tube number). Thus, nearly all exchangeable cations were substituted by Cs^{+} and released in the solution during the first washing cycle. In the case of the Ni-hectorite sample, the concentration of the exchangeable Ni^{2+} cations (0.486 mmol/g) is in very good agreement with the nominal value defined by the layers charge (0.8*e*). The result for the Sm-hectorite sample is different: the concentration of the exchangeable cations (0.242 mmol/g) was found to be less by 32% than that absorbed by the hectorite (0.365 mmol/g).

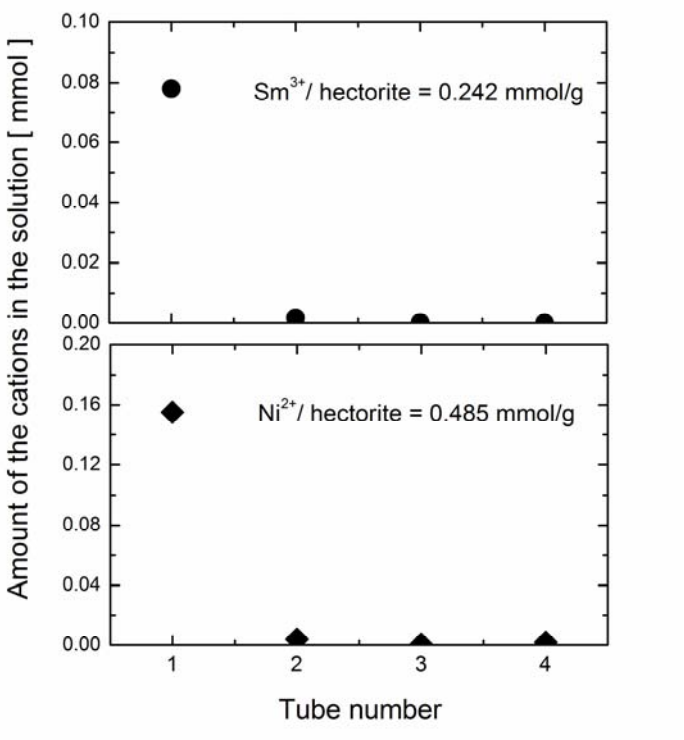

Figure 1. Total amount of Sm^{3+} (top) and Ni^{2+} (bottom) as a function of the tube number (see text for details). The calculated concentrations of exchangeable cations in hectorite (Sm^{3+}/hectorite, Ni^{2+}/hectorite) are indicated in the figure.

3.2 Neutron Scattering Experiments

Previous QENS experiments on hydrated clays have shown that water diffusion mobility is probably a complex dynamical process that cannot be described with the use of a single characteristic time. This is especially true for samples with strongly hydrated interlayer cations like Ni^{2+}, where we expect to find two kinds of water molecules (slow exchange limit): the water molecules hydrating the cation (bound water) and other molecules ("free" water). The diffusion mobility of the bound water molecules is much slower than the mobility of "free" water. This means that we need to perform our measurements with different energy resolutions, which is equivalent to different observation times: with higher resolution we can observe slower mobility of the bound water, whereas the faster mobility of "free" molecules is more visible at lower resolution.

The low-resolution experiment was performed with the TOF spectrometer NEAT at the Berlin Neutron Scattering Center (Helmholtz-Zentrum Berlin). The incident neutron wavelength was $\lambda_0 = 8$ Å, with an elastic resolution $\Delta \sim 30$ μeV measured by using a standard vanadium sample. Flat sample cells with 0.6 mm thickness were used, resulting in a

transmission of about 94%. The sample orientation angle with respect to the incident neutron beam direction was 135°. The QENS was measured in a Q range of 0.23 – 1.33 Å^{-1}.

The high-resolution experiment was carried out on the IN10 back-scattering at the ILL, Grenoble. The incident neutron wavelength was λ_0 = 6.271 Å, with an energy resolution Δ ~1 μeV measured by using a standard vanadium sample. The thickness of flat sample cells was 0.5 mm. Seven detectors were positioned at angles corresponding to average Q values of 0.11, 0.21, 0.29, 0.41, 0.6, 1.18, 1.45 Å^{-1}.

4. Results and Discussion

We analyzed our data using isotropic models for the sake of simplicity, although it has been recently demonstrated that an isotropic approximation can underestimate the diffusion coefficient of the interlayer water molecules [17]. First a preliminary analysis was performed using the simplest models, and some important conclusions were drawn. Then the data for Ni-hectorite and Sm-hectorite were examined in the slow exchange approximation assuming that QENS spectra consist of two components: the bound water component and the "free" water component.

4.1. Preliminary analysis

4.1.1 High resolution data

The QENS spectra measured with IN10 were fitted by the following model (Figure 2):

$$S(Q,\omega) = \left[A(Q)\delta(\omega) + B(Q)\frac{1}{\pi}\frac{\Gamma(Q)}{\Gamma^2(Q)+\omega^2} \right] \otimes R(Q,\omega) \qquad (16)$$

The first term in the brackets (delta function) represents elastic scattering; the second one (Lorentzian) approximates quasielastic scattering. $R(Q,\omega)$ is a resolution function, and $\otimes$ denotes the convolution operation. $A(Q)$ and $B(Q)$ are intensities of elastic and quasielastic scattering, respectively.

The quasielastic fwhm's (= $2\Gamma(Q)$) obtained from the best fit of eq. 16 to the QENS data measured with theIN10 are shown in Figure 3. There are no results for the Na-hectorite at higher Q values, because the QENS spectra become too broad in this Q-region to be measured with the backscattering technique. The fwhm for Na-hectorite shows Q-dependence that is much steeper than for Ni-hectorite and Sm-hectorite; the latter results are very close to each other. This result indicates that Ni^{2+} and Sm^{3+} cations interact with water molecules much stronger than Na^{+}.

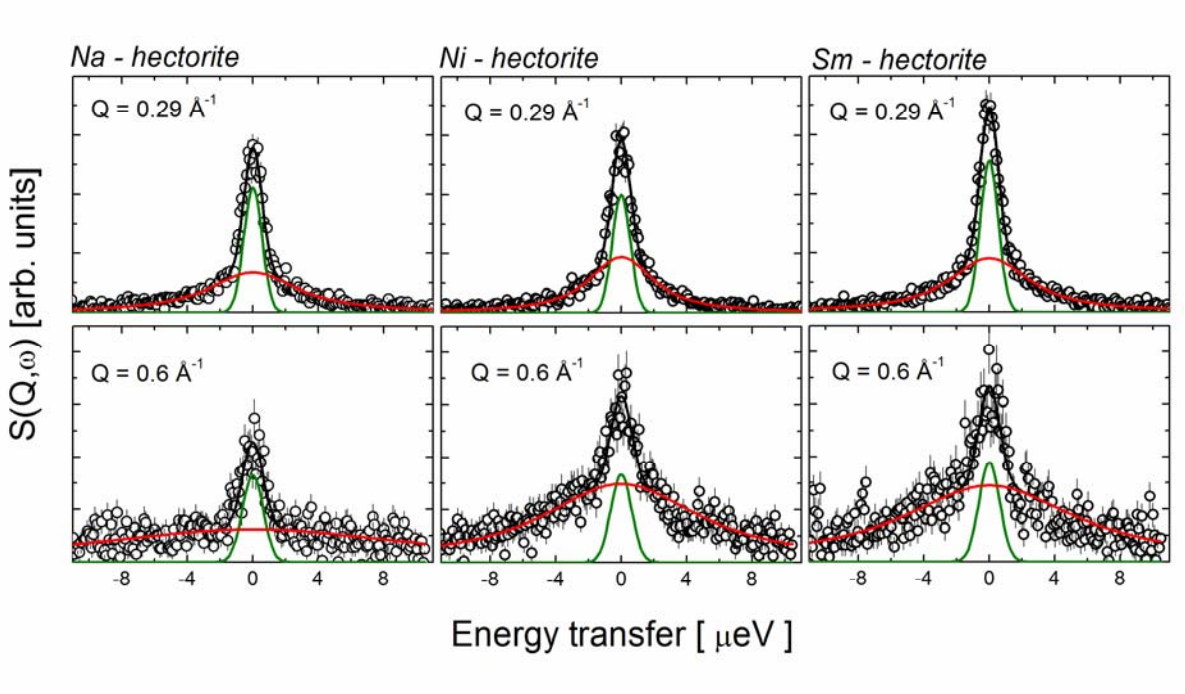

Figure 2. Experimental QENS spectra (circles) measured on the IN10 backscattering spectrometer. Lines: (black) the best fit with eq. 16; (green) elastic scattering; (red) quasielastic scattering.

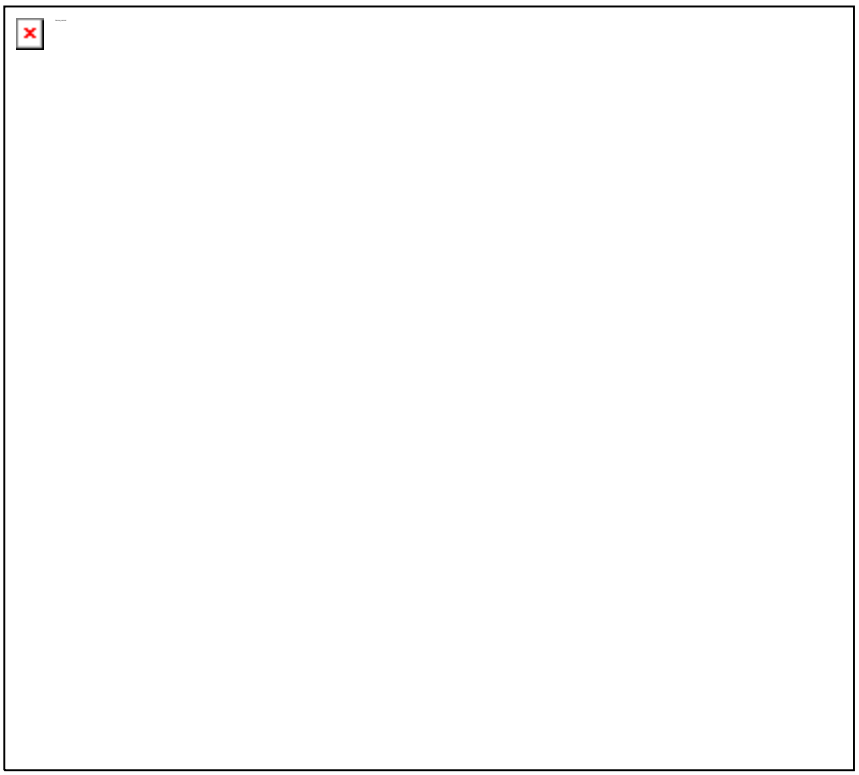

Figure 3. fwhm's of quasielastic scattering (fwhm = $2\Gamma(Q)$) obtained from fitting model (eq. 16) to the experimental spectra measured on the IN10 spectrometer.

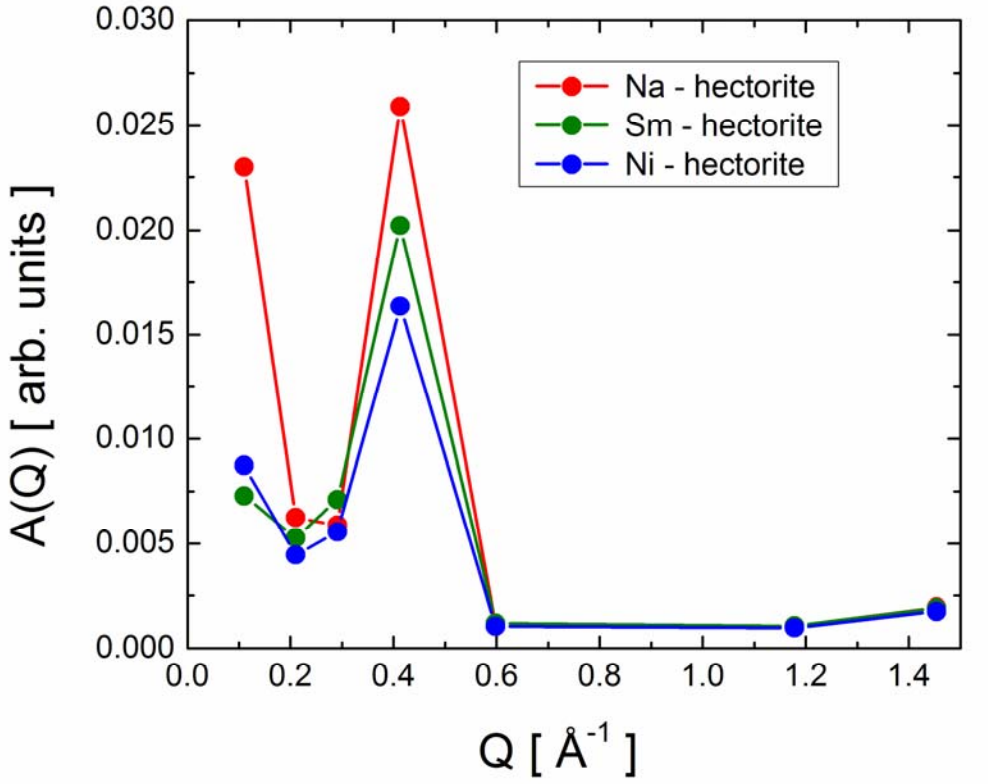

Figure 4. Intensity of elastic scattering *A(Q)* obtained from fitting model 16 to the experimental spectra measured on the IN10 spectrometer.

The elastic scattering intensity *A(Q)* (Figure 4) contains a strong small angle scattering contribution that is much higher for Na-hectorite at $Q = 0.11$ Å^{-1}. This effect can be explained by the difference in the samples preparation: because Na-hectorite sample was synthesized already in the Na-form, no additional treatment was needed; in order to prepare another two hectorite samples we had to saturate them with Sm^{3+} or Ni^{2+} (see Section 3.1 for details). Thus we can suppose that, during preparation of the Sm-hectorite and Ni-hectorite samples (suspension in the solutions, centrifugation, and filtration), we could lose the smaller clay particles or somehow change the pore size distribution in the samples. High elastic intensity at $Q = 0.41$ Å^{-1} is due to the (001) peak corresponding to the interlayer basal spacing (BS).

The *A(Q)* was found to be the same for all three samples except the above mentioned points at $Q = 0.11$ Å^{-1} and 0.41 Å^{-1}. This result is very important, because it indicates that water molecules hydrating Ni^{2+} and Sm^{3+} cations cannot be considered as immobile in our experiment, and the QENS component contains information on their diffusion mobility; otherwise we would have observed an additional elastic scattering in comparison with the Na sample, in which the water molecules hydrating the Na^{+} cation are in fast exchange with "free" water molecules. In the case of Ni^{2+}, the exchange between the bound and "free" water

is extremely slow, and the translation diffusion of the bound water molecules indicated in our experiment must be attributed to the mobility of the whole hydration complex $Ni^{2+}(H2O)_6$. Therefore the diffusion mobility of Ni^{2+} cation in the interlayer of the hectorite is high enough to be measured with the backscattering spectrometer. For the Sm^{3+} cation, the exchange rate between the bound and the "free" water is not known exactly [11]. However, the closeness of the results obtained for the Sm-hectorite and Ni-hectorite samples suggests that the slow exchange approximation is probably applicable to the Sm-hectorite sample as well.

4.1.2 Low resolution data

The position of the (001) reflection, which is visible in the angular dependency of the integral intensity of scattered neutrons measured with the TOF spectrometer (Figure 5), gives the values of the interlayer BS. These values indicate that all three samples are in a two-layer hydrate state. The BS values show dependence on the hydration state of the cation: in the case of the weakly hydrated interlayer Na^+, the BS is significantly smaller than that for the strongly hydrated Ni^{2+}, although the ionic radius of Na^+ is larger (0.98 Å [33]) than that for Ni^{2+} (0.78 Å [33]). The interlayer spacing for Sm-hectorite is larger than that for the two other samples, which is an indication that Sm^{3+} cations in the clay interlayer (at least some of them) form outer-sphere adsorption complexes.

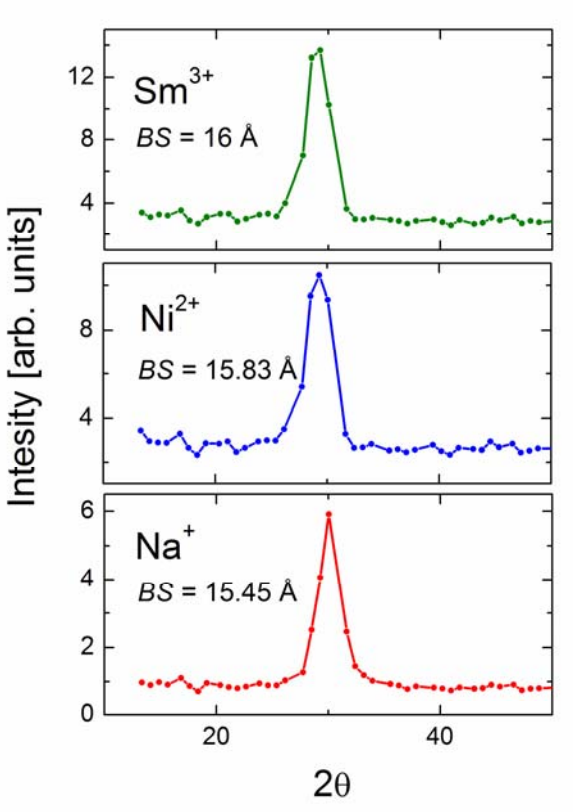

Figure 5. Intensity of scattered neutrons as a function of scattering angle (TOF data). The BS is indicated for each data set.

The QENS spectra, measured for the Na sample, were fitted by two models: model 16, which was used for the analysis of the high resolution data, and the model that takes into account individual reorientations of water molecules:

$$S(Q,\omega) = \left[A(Q)\delta(\omega) + B(Q)\frac{1}{\pi}\frac{\Gamma(Q)}{\Gamma^2(Q)+\omega^2} \otimes S_{rot}(Q,\omega) \right] \otimes R(Q,\omega), \qquad (17)$$

where $S_{rot}(Q,\omega)$ is the rotation scattering law defined by eq. 9 (the first three terms of the expansion), with the radius of rotation R_0 = 1 Å (O-H distance in the water molecule). The other terms of formula 17 are the same as in eq. 16. For the fitting of the low-resolution QENS data by models 16 and 17, we used the results for the elastic intensity $A(Q)$ found from the analysis of the high-resolution spectra (Figure 4) after normalization by the total scattered intensity in the Q range of 0.2 – 0.3 Å^{-1}.

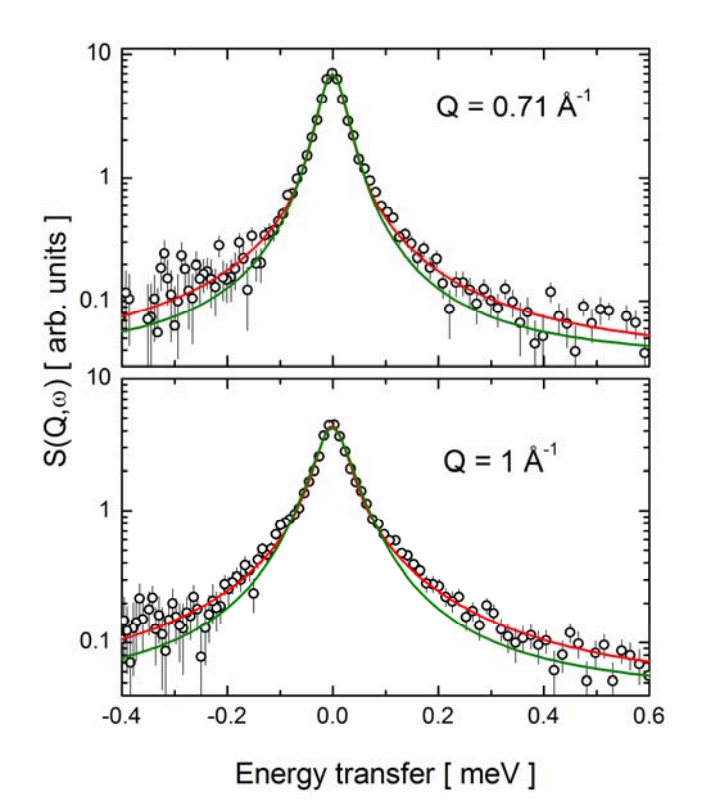

Figure 6. The low-resolution QENS spectra measured for the Na-hectorite sample. Lines: (green) fit by model 16, (red) fit by model 17.

The quality of the fit by model 16 degrades at Q > 0.6 $Å^{-1}$, and model 17 fits the experimental spectra better at these Q values (Figure 6). The rotation diffusion constant was found to be D_r = 0.06 ± 0.02 meV, this value is somewhat lower than that reported for the bulk water at room temperature (D_r ≈ 0.1 meV [34]). The translational diffusion QENS widths (fwhm = $2\Gamma(Q)$) for the Na-hectorite sample are shown in Figure 7. The results obtained using models 16 and 17 are very close to each other for $Q \leq 0.71$ $Å^{-1}$ ($Q^2 < 0.51$ $Å^{-2}$) and can be described by the simple diffusion model 8 with diffusion coefficient D = (0.63 ± 0.03) x 10^{-9} m^2/s. The difference between models 16 and 17 arises at higher Q values, where effect of reorientations becomes important; whereas the result for model 16 is still close to the strait line predicted by the simple diffusion law, the fwhm, obtained using model 17, shows increasingly lower values tending to its high Q^2 limit, as it is supposed by the jumping mechanism of diffusion [18]. However, neither the Singwi-Sjölander [35] nor the Hall-Ross [36] jump diffusion models can fit the experimental data for Na-hectorite with good accuracy (see Figure 7), therefore the water diffusion in the Na-hectorite is probably a more complex process than is supposed by the simple jump diffusion models.

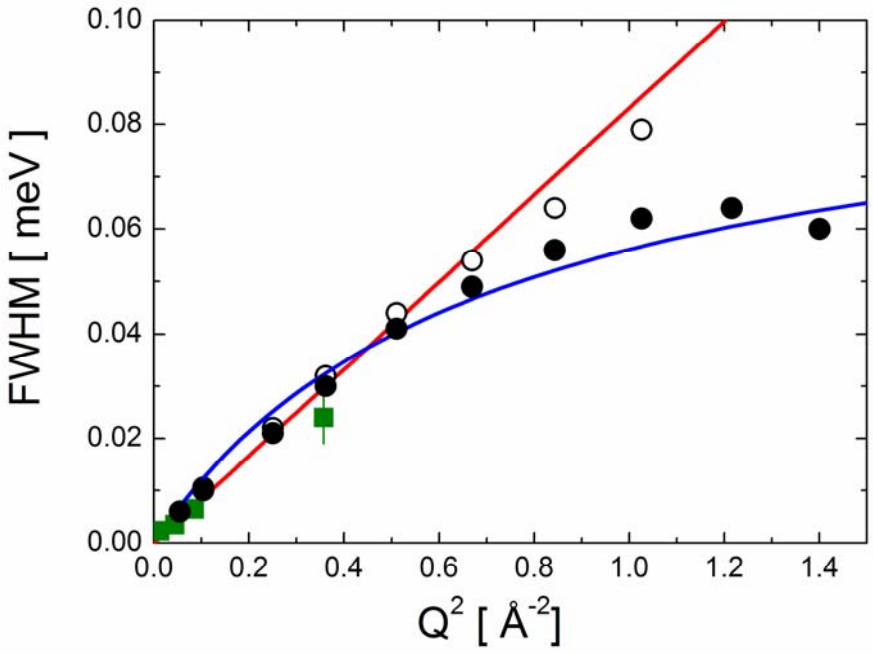

Figure 7. The fwhm of the translational QENS component obtained for Na-hectorite sample with high resolution (green squares) and low resolution (circles). Open circles: model 16, black circles: model 17. Red line represents simple diffusion law (eq. 8). Blue line is a fit by the Hall-Ross model [36].

The agreement between the results for the Na-hectorite sample obtained with the high and low resolutions is good (Figure 7). Unfortunately the quasielastic widths $\Gamma(Q)$ for this sample are measurable with a backscattering spectrometer at low Q ($Q \leq 0.6$ Å^{-1}) only. Malikova et al. [17] reported a good agreement in the relaxation times of water mobility in a synthetic Na-hectorite extracted with the NSE (high resolution) and TOF (low and medium resolutions) techniques in a Q range up to $Q = 1$ Å^{-1} [17] using an approximation equivalent to model 16. Thus the approximation that we use for the data analysis is sufficient for the description of the experimental data obtained for the Na-hectorite sample. Therefore we did not try to fit our QENS spectra using KWW function (eq. 10), which would complicate our analysis of the Sm-hectorite and Ni-hectorite samples.

The obtained water diffusion coefficient $D = (0.63 \pm 0.03) \times 10^{-9}$ m^2/s for the Na-hectorite sample is higher than $D = (0.43 - 0.46) \times 10^{-9}$ m^2/s reported in ref 17 for the same system. One of the reasons for this difference could be some differences in the samples preparation: the water content for the sample described in ref 17, $n(H_2O)/Na^+ = 7.1$, was considerably lower than in our case, $n(H_2O)/Na^+ = 11.5$. Another possible reason is the elastic neutron scattering on clay atoms. The use of a fluorated clay mineral strongly reduces the elastic scattering from the clay layer atoms in comparison to natural clays. However, for the fluorated hectorite, the elastic scattering is small but not negligible: at large Q values, it is of about 5% of the total intensity, but at smaller Q values, it can be much higher as a result of the small angle scattering (Figure 4). In our case, the contribution of the elastic scattering to the total intensity is about 25% at $Q = 0.2$ Å^{-1}. If we ignored the elastic contribution, the water diffusion coefficient estimated with the resolution of our experiment ($\Delta \sim 30$ μeV) would be $D = (0.55 \pm 0.03) \times 10^{-9}$ m^2/s.

The QENS spectra measured for the Ni-hectorite and Sm-hectorite samples were fitted by expression 17. The obtained fwhm of the translational QENS component is shown in Figure 8 together with the data for the Na-hectorite and the high-resolution results. The presented fwhm indicates that water molecules in the Na-hectorite are more mobile than those in the Sm-hectorite and Ni-hectorite samples. The result for the Sm-hectorite is close to that for the Ni-hectorite; this means that interaction between water and Sm^{3+} is strong, and the Sm^{3+} is most probably fully hydrated. Thus our QENS results do not support the previous interpretation of the neutron diffraction experiments that the Sm^{3+} cation forms an inner-sphere complex with the clay surface. The higher mobility of water molecules in the Sm-hectorite sample in comparison to the Ni-hectorite leaves an opportunity for a compromise with the results of the neutron diffraction experiments: it can be supposed that not all

adsorbed Sm^{3+} cations interact with water molecules, probably because of the precipitation. For example, in the Sm hydroxide, the number of oxygen atoms closest to the Sm, N_O = 9, and Sm-oxygen distance, R_{SmO} = 2.47 Å [37], are very similar to the parameters of the first coordination shell of the Sm^{3+} cation in an aqueous solution. This interpretation is supported by our cationic exchange analysis: it was found that 32% of the adsorbed Sm^{3+} cations are not exchangeable.

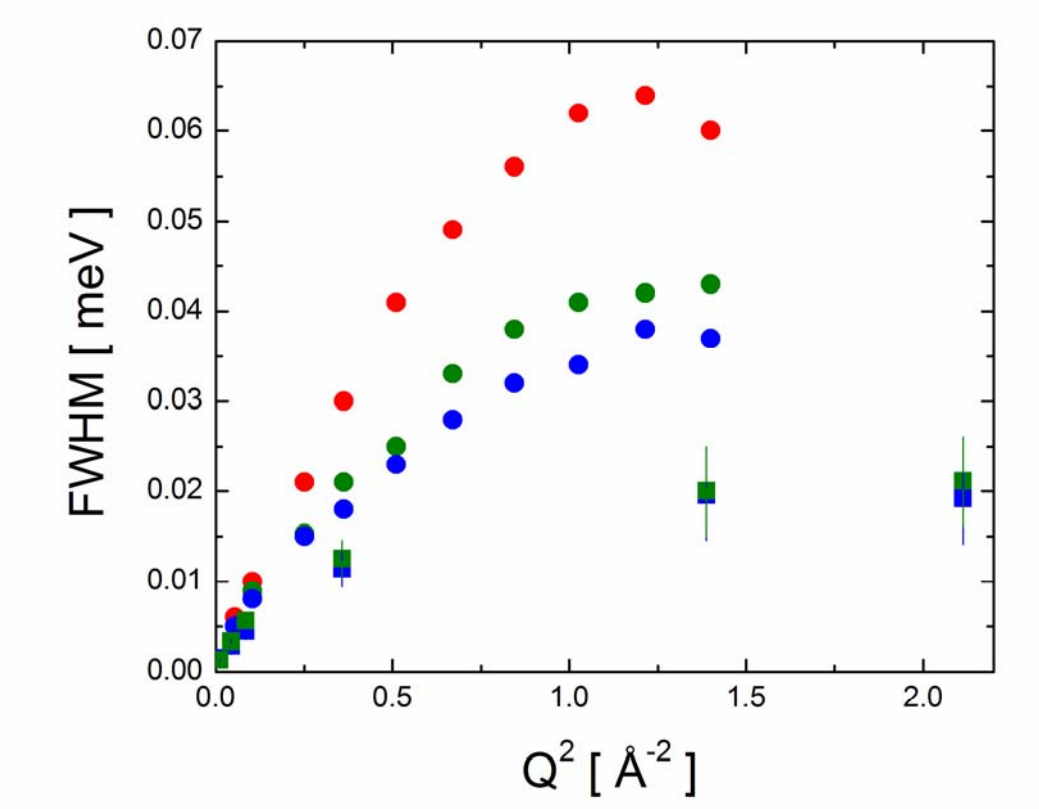

Figure 8. The fwhm of the translational QENS component obtained for the Na-hectorite (red), Sm-hectorite (green), and Ni-hectorite (blue) with high resolution (squares) and low resolution (circles). The high-resolution result for the Na-hectorite sample is shown in Figure 7.

In contrast to the Na-hectorite in the case of Sm-hectorite and Ni-hectorite samples, there is a significant difference between the quasielastic fwhm obtained with high and low resolution (Figure 8). This effect is not surprising because the results shown in Figure 8 are obtained in a single component approximation assuming only one population of water molecules. The fact that this approximation leads to a good agreement between the high-resolution and low-resolution quasielastic widths for the Na-hectorite sample confirms our supposition that the bound and "free" water molecules in this system are in fast exchange. In

the case of Ni-hectorite, the single component approximation is not applicable, because we expect to observe two distinct QENS components corresponding to the bound and "free" water molecules. The high-resolution QENS is more sensitive to the slow motions of the bound water molecules, and the low-resolution data reflects mainly the faster motions of the "free" water molecules. Because the results obtained for the Sm-hectorite look very similar to those for the Ni-hectorite, one can suppose that the slow exchange approximation is likely applicable to the Sm-hectorite sample as well.

4.2. Slow exchange approximation for Ni-hectorite and Sm-hectorite

The aim of the further analysis is to determine the diffusion coefficients of the interlayer cations Ni^{2+} and Sm^{3+} supposing that these cations diffuse together with their hydration shells. Because of complexity of the studied systems and some deficit of the experimental data measured with high resolution, we can only make some rough estimations.

First the QENS spectra for the Ni-hectorite were fitted by the following model (Figure 9):

$$S(Q,\omega) = \left[A(Q)\delta(\omega) + B(Q)(\alpha S_{bound}(Q,\omega) + (1-\alpha) S_{free}(Q,\omega))\right] \otimes R(Q,\omega), \quad (18)$$

where α is the fraction of the bound water molecules. $S_{bound}(Q,\omega)$ and $S_{free}(Q,\omega)$ are the QENS components for the bound and "free" water molecules respectively. The other terms in expression 18 are the same as those in 16 and 17.

The $S_{free}(Q,\omega)$ was modeled in the same way as before:

$$S_{free}(Q,\omega) = \frac{1}{\pi} \frac{\Gamma_{free}(Q)}{\Gamma_{free}^2(Q) + \omega^2} \otimes S_{rot}(Q,\omega)$$

where $S_{rot}(Q,\omega)$ is a rotational scattering law, the same as in model 17. It should be noted that effect of individual rotations of water molecules is only important at $Q > 0.6$ Å^{-1} and only for the low-resolution analysis, because such rotations are too fast to be detected with a backscattering spectrometer.

In the first approximation $S_{bound}(Q,\omega)$ was expressed as:

$$S_{bounde}(Q,\omega) = \frac{1}{\pi} \frac{\Gamma_{bound}(Q)}{\Gamma_{bound}^2(Q) + \omega^2} \quad (19)$$

Only the parameters $B(Q)$, $\Gamma_{free}(Q)$ and $\Gamma_{bound}(Q)$ were varied in the fitting procedure. For $A(Q)$ and parameters of $S_{rot}(Q,\omega)$, the values found from the preliminary analysis were used. For six water molecules hydrating Ni^{2+}, α = 0.25. The fitting procedure was iterative: when the high-resolution data was fitted, $\Gamma_{free}(Q)$ was kept fixed, using the value obtained

from the low-resolution analysis. And, vice versa, fitting the low-resolution spectra, we used, in the same way, the high-resolution result for $\Gamma_{bound}(Q)$.

The result of the fit, fwhm = $2\Gamma_{bound}(Q)$, is shown in Figure 10. Unfortunately, only four Q values are now available. The spectra at Q = 0.11 Å^{-1} and 0.41 Å^{-1} were not fitted because of the strong elastic scattering (the small angle scattering and (001) peak). The spectrum at Q = 1.45 Å^{-1} (Q^2 = 2.11 Å^{-2}) was also excluded from the analysis, because the low-resolution data was not available at this Q value, and, therefore, a separation of $S_{bound}(Q,\omega)$ and $S_{free}(Q,\omega)$ was hardly possible. The fit of the first three points with the simple diffusion model 8 gives the three-dimensional (3D) diffusion coefficient of the Ni^{2+} cation in the hectorite interlayer space: D_{Ni} = (0.12 ± 0.02) x 10^{-9} m^2/s. However, this value is only a high limit estimation of D_{Ni}, because expression 19 does not take into account rotation diffusion.

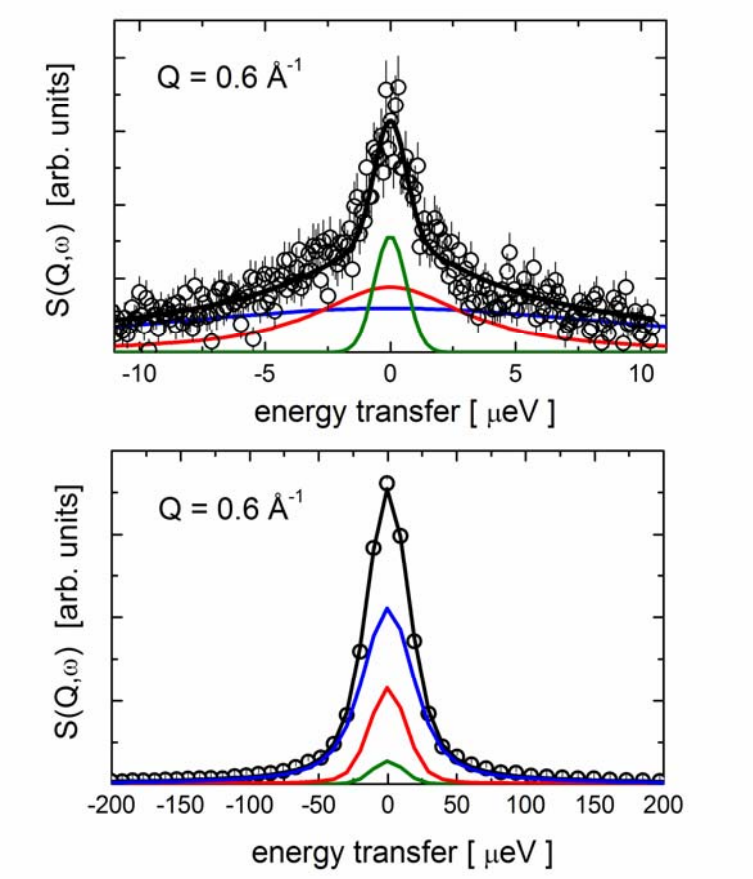

Figure 9. The QENS spectra for the Ni-hectorite sample measured with high resolution (top) and low resolution (bottom). Curves: (black) the fit by model 18; (green) elastic scattering; (red) bound water component; (blue) "free" water component.

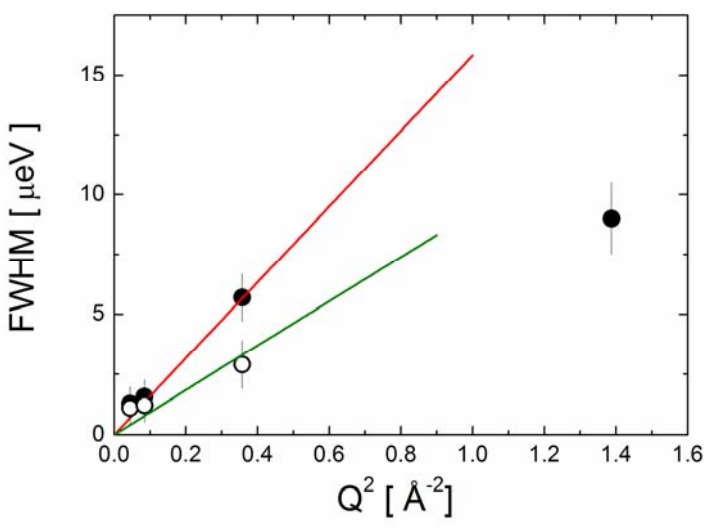

Figure 10. The fwhm of the $S_{bound}(Q,\omega)$ component for the Ni-hectorite sample: the result of the fit using model 19 (black circles); the result of the fit using model 20 with Δ_{rot} = 4.5 μeV (open circles). Lines represent a fit by model 8.

In a simplified form, taking into account rotation effects, the $S_{bound}(Q,\omega)$ can be expressed as (see eqs. 6, 7b, and 9):

$$S_{bound.}(Q,\omega) \approx EISF(Q)\frac{\Gamma_{bound}(Q)}{\Gamma_{bound}^2(Q)+\omega^2} + (1-EISF(Q))\frac{\Gamma_{bound}(Q)+\Delta_{rot}}{\left(\Gamma_{bound}(Q)+\Delta_{rot}\right)^2+\omega^2}, \qquad (20)$$

where Δ_{rot} is the rotational quasielastic width.

The structure factors $EISF(Q) = j_0^2(QR_0)$, calculated using the isotropic approximation 9, for isolated rotations of water molecules and reorientation of the hydration complex $Ni^{2+}(H_2O)_6$ are plotted in Figure 11. The radius of rotation R_0 = 1 Å (O-H distance in the water molecule) was used to calculate the EISF(Q) for the isolated rotations of water molecules; for the rotational radius of the $Ni^{2+}(H_2O)_6$ complex we used the Ni – H distance R_0 = 2.7 Å found in neutron diffraction experiments on aqueous solutions and hydrated Ni-montmorillonite [9]. The individual rotations of water molecules cannot considerably affect our results, at least at Q^2 values less than 0.4 Å^{-2}, even if we suppose that this rotations are much slower than in bulk water, because at these Q values EISF(Q) >0.85 and the $S_{bound}(Q,\omega)$ is dominated by the first term of eq. 20. However the reorientation of the hydration complex $Ni^{2+}(H_2O)_6$ can be visible even at low Q values.

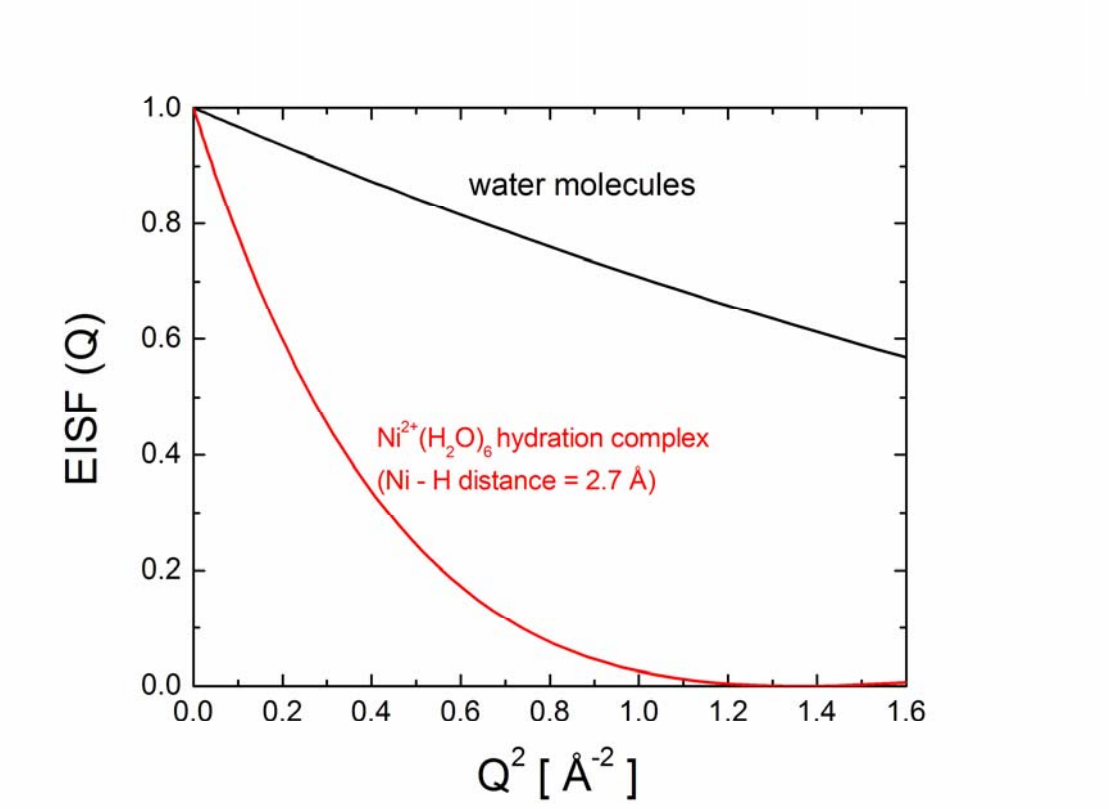

Figure 11. The structure factors EISF(Q) = $j_0^2(QR_0)$ for individual rotations of water molecules (black) and for the reorientation of the hydration complex $Ni^{2+}(H_2O)_6$.

The reorientation correlation time τ_1 of the hydration complex $Ni^{2+}(H_2O)_6$ in an aqueous solution calculated by molecular dynamics (MD) simulation was found to be τ_1 =150 ps [38]. The corresponding quasielastic width, fwhm = $2\hbar/\tau_1 \approx 9$ μeV, is very close to the $fwhm_{bound}$ shown in Figure 10 at Q^2 =1.39 Å^{-2}, where the first term of eq. 20 vanishes (Figure 11). On the other hand, a hypothesis that the observed quasielastic signal from the bound water molecules is purely rotational is not consistent with our experimental data: model 18 with $S_{bound}(Q,\omega)$ defined by model 20, and the parameter $\Gamma_{bound}(Q)$ = 0 does not fit the high-resolution QENS spectra (see Figure 12).

The accuracy of our high-resolution data does not allow us to introduce another fitting parameter. Nevertheless, one can estimate the lower limit of $\Gamma_{bound}(Q)$. It was already mentioned above that, at Q^2 =1.39 Å^{-2}, the second term of eq. 20 dominates (Figure 11). The fwhm value at Q^2 =1.39 Å^{-2} was used as an upper limit estimation for the rotational width Δ_{rot}

$$FWHM(Q^2 = 1.39) \approx 2(\Delta_{tr} + \Delta_{rot}) \approx 2\Delta_{rot} \qquad (21)$$

The fit of the high-resolution data at Q = 0.21 Å^{-1}, 0.29 Å^{-1} and 0.6 Å^{-1} by models 18 and 20 with Δ_{rot} estimated from eq. 21 (Figure 12) gives the low limit estimations for the

$\Gamma_{bound}(Q)$ and the diffusion coefficient of the Ni^{2+} cation: D_{Ni} = (0.07 ± 0.02) x 10^{-9} m^2/s (Figure 10).

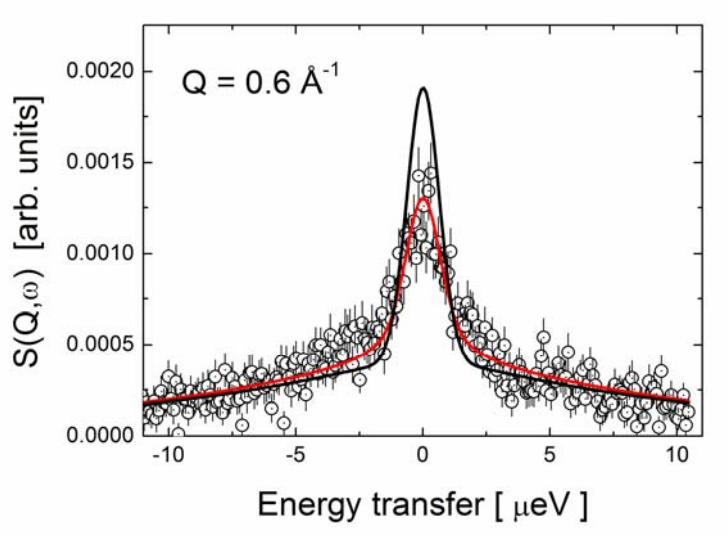

Figure 12. The high-resolution QENS for the Ni-hectorite sample (circles) fitted with models 18 and 20 using the following constrains: $\Gamma_{bound}(Q)$ = 0, Δ_{rot} is a fitted parameter (black line); Δ_{rot} = 4.5 μeV, $\Gamma_{bound}(Q)$ is a fitted parameter (red line). The EISF(Q) = $j_0^2(QR_0)$ is calculated using R_0 = 2.7 Å (see the text for details).

Thus, the upper and lower limit values for D_{Ni}, taking into account the error bars, give the estimation of the diffusion coefficient of the Ni^{2+} cation in the interlayer of the hectorite: D_{Ni} = (0.05 – 0.14) x 10^{-9} m^2/s.

The QENS spectra for the Sm-hectorite sample were analyzed in the same way as the Ni-hectorite data, but for two cases:

a) All adsorbed Sm^{3+} cations interact with water molecules. In this case the fraction of the bound water molecules is α = 0.27.
b) Only half of the adsorbed Sm^{3+} interact with water molecules, as it follows from the neutron diffraction experiments, α = 0.135.

A distance of R_0 = 3.1 Å for Sm-H correlation, as obtained from neutron diffraction experiments [4-6], was used in the EISF(Q) calculation for the rotation of the hydrated $Sm^{3+}(H_2O)_8$ complex. Unfortunately, the statistical accuracy of our high-resolution data is not good enough to give a preference to one of the above cases from the goodness of fit. The quality of the fit of the experimental QENS is approximately the same for both cases. In case (b) (α = 0.135), the smaller contribution of the $S_{bound}(Q,\omega)$ component is compensated by the

weak narrowing of the $S_{free}(Q,\omega)$ component (by ~ 10 %) and by the strong decrease of the $S_{bound}(Q,\omega)$ width $\Gamma_{bound}(Q)$. The fwhm of $S_{bound}(Q,\omega)$ for both cases is plotted in Figures 13 and 14, and the estimated values of the diffusion coefficients for the Sm^{3+} cation are shown in Table 1. The D_{sm} values found for case (a) are slightly higher than D_{Ni}, while in case (b) it is $D_{Sm} < D_{Ni}$. The result for case (b) looks more realistic, because the Sm^{3+} cation is larger than Ni^{2+}, and it is hydrated by a larger number of water molecules, therefore its diffusion mobility should be slower.

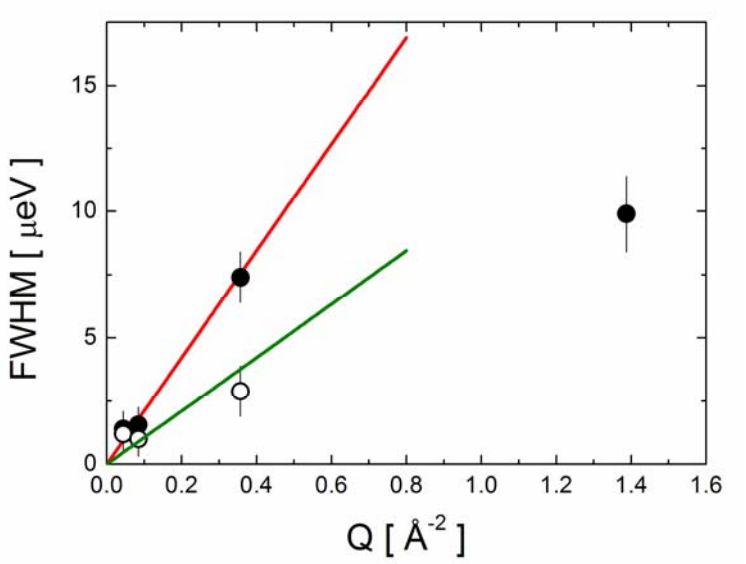

Figure 13. The fwhm of the $S_{bound}(Q,\omega)$ component for the Sm-hectorite sample obtained with α = 0.27: the result of the fit using model 19 (black circles); the result of the fit using model 20 with Δ_{rot} = 4.9 μeV (open circles). Lines represent a fit by model 8.

For the first time the diffusion mobility of strongly hydrated interlayer cations have been measured by QENS. The previous QENS study of the rotational and translational diffusional dynamics of water in Ca^{2+}- and Mg^{2+}-exchanged montmorillonite carried out by Tuck et al. [23] with a similar experimental setup found no evidence of the diffusion mobility of the water molecules hydrating interlayer cations, although Mg^{2+}, like Ni^{2+}, is very strongly hydrated. The MD simulation performed for Mg-beidellite [39] also showed that, over the time scales of the simulations (500-1175 ps), the solvated Mg^{2+} cations remain in fixed locations near negative charge sites within the clay layers. Natural montmorillonite and beidellite clay minerals used for those studies are clays with tetrahedral substitutions, whereas the synthetic hectorite that we probed in our experiments contains only octahedral substitutions. Therefore, our results indicate that interlayer cations are more mobile in clays

with octahedral substitutions than in clays with tetrahedral ones, where negative charge sites locate closer to the layer surface.

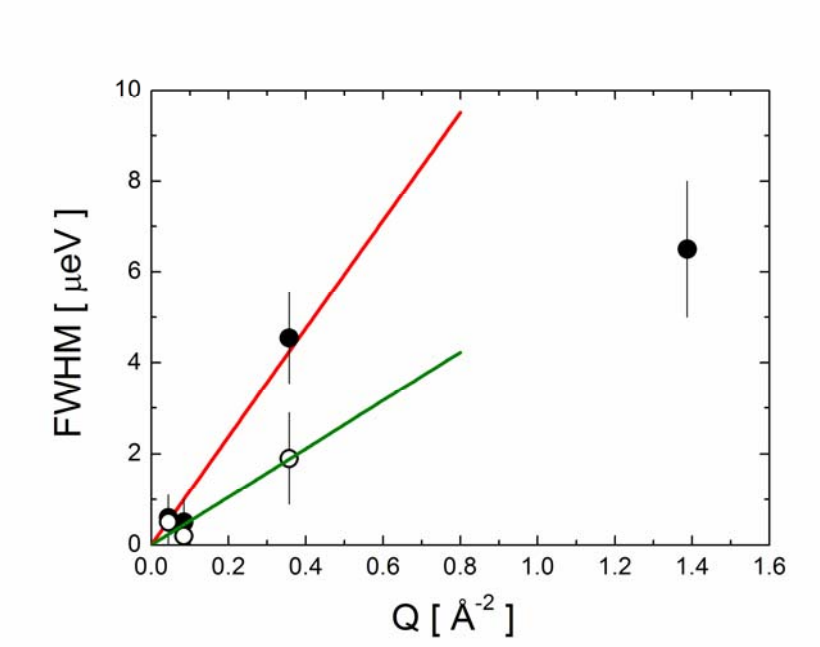

Figure 14 The fwhm of the $S_{bound}(Q,\omega)$ component for the Sm-hectorite sample obtained with α = 0.135: the result of the fit using model 19 (black circles); the result of the fit using model 20 with Δ_{rot} = 3.3 μeV (open circles). Lines represent a fit by model 8.

Table 1. Diffusion coefficients of Ni^{2+} and Sm^{3+} obtained for different values of the parameter α (Fraction of the bound water molecules)

Cation	α	D_{ion} x 10^{-9} m^2/s
Ni^{2+}	0.25	0.05 – 0.14
Sm^{3+}	0.27	0.06 – 0.18
	0.135	0.04 – 0.11

The QENS method, with the use of fluorated clay, is very promising for the study of hydration of clay interlayer cations. Not only diffusion coefficients but also coordination numbers can be estimated. In the case of the present study, the obtained information is not very detailed because of the lack of experimental data measured at high resolution: only spectra measured by seven detectors were available, and the statistical accuracy was also poor. More detailed results could be achieved with the use of more modern backscattering spectrometers, such as IN16 (ILL), SPHERES (FRM-2), or BASIS (SNS). The combination

of MD simulations with experimental results would also be very helpful for the interpretation of the latter.

5. Conclusion

QENS experiments were performed with Na-hectorite, Ni-hectorite, and Sm-hectorite samples in order to compare the results obtained for Sm^{3+} with other interlayer cations: strongly hydrated Ni^{2+} and relatively weakly hydrated Na^{+}. It was found that water mobility in the Sm-hectorite sample is very close to the water mobility in the Ni-hectorite. This is only possible if the Sm^{3+} ion is fully hydrated. A compromise with the neutron diffraction data can be found, assuming that not all adsorbed Sm interacts with water molecules, probably due to precipitation. This is supported by the cationic exchange experiment.

It was shown that water molecules hydrating Ni^{2+} and Sm^{3+} exhibit diffusion mobility measurable with backscattering spectrometers. The diffusion coefficients of the exchangeable cations were found using the slow exchange approximation to be D_{Ni} = (0.05 – 0.14) x 10^{-9} m^2/s and D_{Sm} = (0.04 – 0.18) x 10^{-9} m^2/s.

Acknowledgment.

We gratefully acknowledge financial support from the EURATOM (Contract No. 044806: "Hydration and Hydrolysis of Exchangeable Radionucleides in Clays"). This research project has been supported by the European Commission under the 6th Framework Programme through the Key Action: Strengthening the European Research Infrastructures. Contract No. RII3-CT-2003-505925 (NMI 3). L. Le Forestier thanks the French national research agency (ANR) for financial support of synthesis equipment (project ANR-07-JCJC-0013-01).

Supporting Information Available: Simple model for fast and slow exchange limits of QENS**.** This material is available free of charge via the Internet at http://pubs.acs.org.

References and Notes

1. Sposito, G.; Skipper, N.T.; Sutton, R.; Park, S.-H.; Soper, A.K.; Greathouse, J.A. *Proc. Natl. Acad. Sci. U.S.A.* **1999**, 96, 3358-3364.
2. Bradbury, M.H.; Bayens, B. *Geochim. Cosmochim. Acta* **2002**, 66, 2325-2334.
3. Pitteloud, C.; Powell, D.H; Gonzalez, M.A.; Cuello, G.J. *Colloids and Surfaces A: Physicochem. Eng. Aspects* **2003**, 217, 129-136.

4. Sobolev, O.; Charlet, L.; Cuello, G. J.; Gehin, A.; Brendle J.; Geoffroy, N. *J. Phys.: Condens. Matter.* **2008**, 20, 104207.
5. Sobolev, O.; Charlet, L.; Cuello, G.J.; Gehin, A.; Brendle, J. *Radiochem. Acta* **2008**, 96, 1–5.
6. Sobolev, O.; Charlet, L.; Cuello, G.J. ILL Experimental Report, Prop. No 6-05-742
7. Slade, P. G.; Self, P. G. and Quirk J. P. *Clays Clay Minerals* **1998**, 46, 629–635.
8. Kowal-Fouchard, A.; Drot R.; Simoni, E.; Marmier, N.; Fromagec, F. and Ehrhardt, J-J; *New J. Chem.* **2004**, 28, 864–869.
9. Pitteloud, C.; Powell, D. H.; and Fischer, H. E. *Phys. Chem. Chem. Phys.* **2001,** 3, 5567-5574.
10. Smith, D.W. Inorganic Substances: A Prelude to the Study of Descriptive Inorganic Chemistry; Cambridge University Press: Cambridge, U.K., 1990.
11. Salmon, P. S.; Howell W. S.**;** Mills R. *J. Phys. C: Solid State Phys.* **1987**, 20, 5727-5747.
12. Hunt, J. P.; Friedman, H. L. *Prog. Inorg. Chem.* **1983**, 30, 359.
13. Impey, R. W.; Maden, P. A.; McDonald, I. R. *J. Phys. Chem.* **1983***,* 87, 5071.
14. Koneshan, S.; Rasaiah, J. C.; Lynden-Bell, R. M.; Lee S. H. *J. Phys. Chem. B* **1998,** 102, 4193-4204.
15. Malikova , N.; Cadene, A.; Marry, V.; Dubois, E.; Turq, P.; Zanotti, J.-M.; Longeville S. *Chemical Physics* **2005**, 317, 226–235.
16. González, F.; Jurányi, F.; Van Loon, L.; Gimmi, T. *Eur. Phys. J. Special Topics* **2007,** 141, 65–68.
17. Malikova, N.; Cadene, A.; Dubois, E.; Marry, V.; Durand-Vidal, S.; Turq, P.; Breu, J.; Longeville, S.; Zanotti, J.-M. *J. Phys. Chem. C* **2007**, 111, 17603-17611.
18. Bee, M. *Quasielastic Neutron Scattering: Principles and Applications in Solid State Chemistry, Biology and Materials Science,* Adam Hilger, Bristol, 1988.
19. Bee, M. *Chemical Physics* **2003**, 292, 121–141.
20. Cummins, H.Z.; Gen, Li.; Hwang, Y.H.; Shen, G.Q.; Du, W.M.; Hernandez, J.; Tao, N.J.Z. *Phys. B* **1997**, 103, 501–519.
21. Arbe, A.; Colmenero, J.; Monkenbusch M.; Richter, D. *Phys. Rev. Lett.* **1998**, 81, 590-593.
22. Sobolev, O.; Novikov, A.; Pieper, J. *Chem. Phys.* **2007**, 334, 36-44.
23. Tuck, J.J.; Hall, P.L.; Hayes, M.H.B.; Ross, D.K.; Poinsignon, C. *J.Chem. Soc., Faraday Trans.* **1984,** 80, 309.
24. Cebula, D.J.; Thomas, R.K.; White, J.W. *Clays Clay Miner.* **1981**, 29, 241.

25. Swenson, J.; Bergman, R.; Howells, W.S. *J.Chem.Phys.* **2000**, 113, 2873.

26. Swenson, J.; Bergman, R.; Longeville, S. *J.Chem.Phys.* **2001**, 115, 11299.

27. Swenson, J.; Howells, W.S. *J. Chem. Phys.* **2002**, 117, 857.

28. Mamontov, E. *J. Chem. Phys.* **2004**, 121, 9193.

29. Marry, V.; Malikova, N.; Cadene, A.; Dubois, E.; Durand-Vidal, S.; Turq, P.; Breu, J.; Longeville, S.; Zanotti, J.-M. *J.Phys.: Condens. Matter* **2008**, 20, 104205.

30. Salmon, P.S. *J. Phys. C: Solid State Phys.,* **1987**, 20, 1573-1587.

31. Gerstmans, A.; Urbanczyk, L.; Jérôme, R.; Robert, J.L.; Grandjean, J. *Clay Min*., **2008**, 43, 205-212.

32. Hamilton, D.L.; Henderson, C.M.B. *Mineral. Mag.* **1968**, 36, 832-838.

33. Emsley, J. The Elements; Oxford University Press: New York, 2000.

34. Teixeira, J.; Bellissent-Funel M.-C.; Chen, S. H.; Dianoux, A. J.; *Phys. Rev. A* **1985**, 31, 1913-1917.

35. Singwi K. S. and Sjolander A. *Phys. Rev.* **1960**, 119, 863-871.

36. Hall P. L. and Ross D. K. *Mol. Phys.* **1981**, 42, 673-682.

37. Milligan, W.O.; Mullica, D.F.; Oliver, J.D. *J. Appl. Crystallogr*. **1979**, 12, 411-412.

38. Egorov, A.A.; Komolkin, A.V.; Lyubartsev, A.P.; Laaksonen, A. Theor. Chem. Acc. **2006**, 115, 170-176.

39. Greathouse, J.A.; Refson, K.; Sposito, G. *J. Am. Chem. Soc.* **2000**, 122, 11459-11464.